南華大學科技學院永續綠色科技碩士學位學程

碩士論文

Master Program of Green Technology for Sustainability

College of Science and Technology

Nanhua University

Master Thesis

應用有限元素法及室內實驗於深層崩塌之模擬

Using Finite Element Method and Laboratory Experiment on the Deep Seated Landslide Modelling

魏韋

Vivek Kumar

指導教授：洪耀明 博士

Advisor: Yao-Ming Hong, Ph.D.

中華民國 109 年 6 月

June 2020

南 華 大 學

科技學院永續綠色科技碩士學位學程

碩 士 學 位 論 文

應用有限元素法及室內實驗於深層崩塌之模擬

Using Finite Element Method and Laboratory Experiment on the Deep Seated Landslide Modelling

研究生：Jiwan kumar

經考試合格特此證明

口試委員：

指導教授：

系主任(所長)：

口試日期：中華民國 109 年 6 月 29 日

ACKNOWLEDGEMENT

At first, I would like to thank my thesis advisor, Professor Yao-Ming Hong, Associate Professor, Master Program of Green Technology for Sustainability, Nanhua University, Taiwan. The door to Professor Hong's office was always open whenever I ran into a trouble spot or had a question about my research or writing. He has always allowed this paper to be my work and steered me in the right direction whenever he thought I needed it.

I would also like to acknowledge Professor Chen Bo-Ching, Professor Department of Green Technology for Sustainability and Dean. Office of Academic Affairs, Nanhua University, Taiwan as the second reader of this thesis, and I am gratefully indebted to his for his very valuable comments on this thesis.Finally, I must express my very profound gratitude to my parents and my friends and classmates for providing me with unfailing support and their continuous encouragement throughout my years of study and throughout the process of researching and writing of this thesis. This accomplishment wouldn't have been possible without them.

Author

Vivek Kumar

Department of Green Technology for Sustainability

Nanhua University, Taiwan, R.O.C.

中文摘要

本研究乃應用室內實驗及數值方法模擬深層崩塌，首先發展基於無限邊坡理論及達西定律知有限元素法，再由室內實驗推得控制方程式之相關物理參數，例如凝聚力、內摩擦角及滲透係數，並以砂箱進行小尺度之崩塌試驗，並紀錄崩塌過程之位移、孔隙水壓增加及土壓力降低數據，實驗數據並用來修正數值模式，修正之數值模式，將可提供實際現場應用。

關鍵詞：深層崩塌、孔隙水壓、數值方法

ABSTRACT

This study simulated a deep-seated landslide by laboratory experiment and numerical model. A finite element method based on Infinite Slope theory and Darcy's law was developed. Physical parameters including cohesion force, internal friction angle and permeable coefficient to be used in the governing equations of the numerical model were also obtained by laboratory experiments. The experiments were conducted in a setup called sand-box to create a small scale of a landslide in our laboratory. The process related to the landslide movement, the increase in pore-water pressure and the decrease of soil pressure during failure were recorded. The outcome of the landslide experiment was used to calibrate the numerical methods for future applications in the field case.

Keywords: Deep-seated landslide, pore-water pressure, numerical method

TABLE OF CONTENT

LIST OF FIGURE

LIST OF TABLE

Chapter 1 Preface

1.1 Introduction

Landslide is a common phenomenon in almost every part of the world. A landslide is typically known to appear on the hillslope which consist of loose or soft soil like gravel materials. There are two types of hillslope landslides- shallow and deep catastrophic failures. Shallow landslide is mostly triggered by precipitation so that earth and gravel covering the surface will flow along the slopes. Landslides triggered by rainfalls mainly occur in mountainous regions. Some of these landslides occur suddenly and travel at a very high speed and can pose a threat to life and property (Iverson, R. M.,2000). Failure of the slopes can be caused by a high groundwater level or seepage during a long period. Some natural causes can also add to the internal slope failure like piping and even earthquake. In the past years, much researches has been done and many are still going on to prevent and improve the stability of hill slope to avoid disasters (Hsueh-Chun Lin et al, 2015). Among rainfall-induced landslides, fluidized landslides are most often dangerous and damaging based on the occurrence unexpectedly. Generally speaking, rainfall-induced landslides are caused by increased pore pressures and seepage forces during periods of intense rainfall (Prancevic, J. P. et al, 2018). Increased pore pressure decreases the effective stress

in the soil and thus reduces the soil shear strength, eventually resulting in slope failure. Water infiltration results in an increase in the water content and a reduction in the stability of the soil. This results in a decrease in the effective stress near the surface soil and ultimately leading to slope failure. (B.-G. Chae et al, 2015. Failure of the earth materials results in the sliding of soil mass under shear stress. So it can be said that the initiation of the process involves (a) factors contributing to the reduction in shear strength and (b) factors contributing to the increase in shear stress. Addition of water is one of the single-action which may contribute to both in increase in shear stress and a decrease in shear strength (Varnes, D. J.,1978).

In this study, a small landside is simulated in our laboratory in a setup called a sandbox. A sandbox is a modelling technique has been widely used in the research field. The whole process related to a landslide and different parameters like the increase in pore-water pressure and the decrease of soil pressure during failure were recorded. To record the parameters like soil pressure and water pressure an embedded system was developed in which total six numbers of sensors were connected. At last, all the data received were used to calibrate the numerical model developed.

1.2 Objective

The main objective of this paper is to simulate and analyse the soil properties. A finite element method (FEM) is developed based on the theory of the Infinite slope and Darcy's Law. This study further aims to analyse the soil properties of all types, mainly the behaviour and deformation in the particular soil mass when the pore water pressure rises in that particular soil.

The investigation was done in COMSOL Multiphysics^{TM} software. FEM was used to simulate the whole geotechnical deformation.

Chapter 2 Literature Review

2.1 Cohesive strength and Internal friction

Properties of Soil:

Small soil particles are held together to form a soil mass because between every soil particles, some internal forces are acting and the offer resistance and resist sliding along any plane. Two of the internal forces are:

- Cohesive strength (c)
- Internal friction (ϕ)

Determination of soil properties (shear strength):

These shear strength parameters can be obtained in the laboratory by three differ types of tests. Tri-axial test, direct shear test and unconfined compression test. The parameters used in this particular study was determined using the tri-axial test.

Tri-axial test:

The soil sample taken for the study was cased inside a very thin rubber membrane and is placed inside of the chamber of the tri-axial test apparatus. The chamber is filled with water and is under constant pressure. The soil sample is loaded with axial load which caused axial stress. The increased axial stress is increased till the sample fails. A very small deformation ($\Delta\sigma$) is measure by the

dial gauge. The sample is put under constant pressure (σ_1) from all sides as shown in the figure.

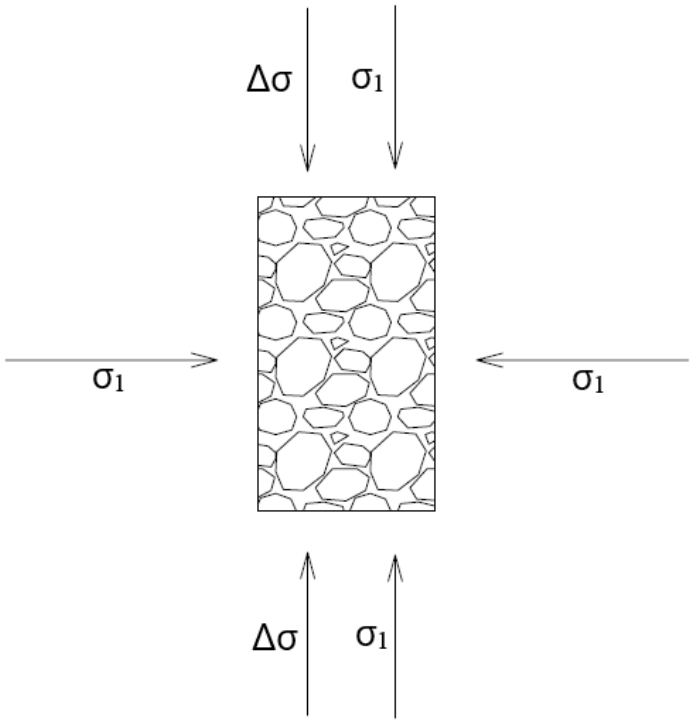

Figure 2-1: Stress application

Where,

Δσ = deformation measured by dial gauge

σ_1 = water pressure from all directions

σ = Total axial stress a failure

therefore, $\sigma = \sigma_1 + \Delta\sigma$

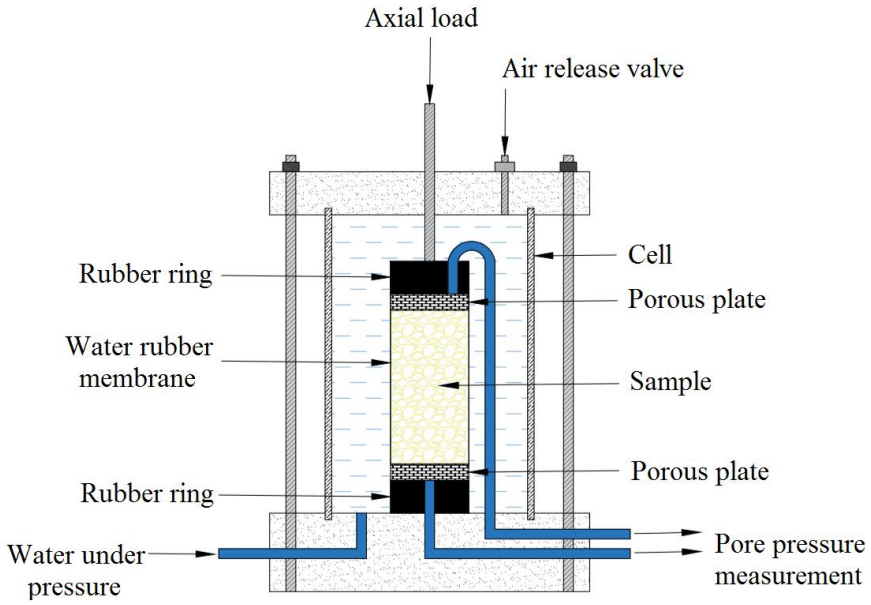

Figure 2-2: Tri-axial test apparatus

In tri-axial test σ and σ_1 are major and minor principal stress respectively. With the major and minor principal stress at failure the following failure envelope is obtained (Figure 2-3)

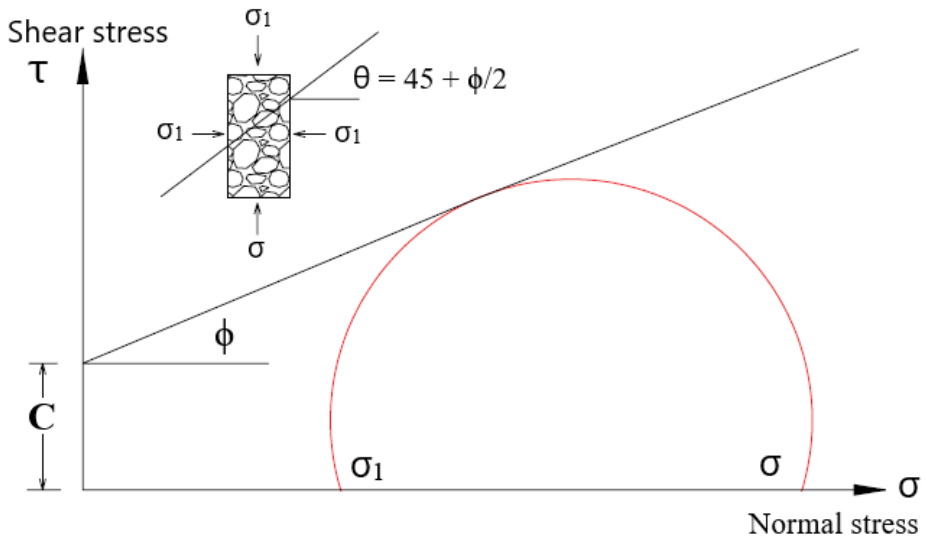

Figure 2-3: Mohr's circle

From the figure 2-2, the angle of failure with the major principal plane is

$$\theta = 45 + \phi/2$$

where, ϕ = angle of internal friction

Therefore, the shear strength equation is

$$S = C + \tan \phi$$

2.2 Mohr's circle

Whenever we consider stress boundary condition it can be represented by a Mohr circle. Mohr's circle is extensively used in the engineering field. It represents a graphical representation to relate stresses on the surfaces oriented to the principal stress. Here in this particular paper, it is used to define two parameters, cohesion (c) and internal frictional angle (ϕ).

The concept can be easily understood by taking an example. As in the figure we consider a surface inclined at an angle θ to the principal stress directions. Here we need to find out the magnitude of the stresses normal and parallel to the surface. Further solving the equations, this will give the graph leading to the Mohr's circle. (Figure 2-3)

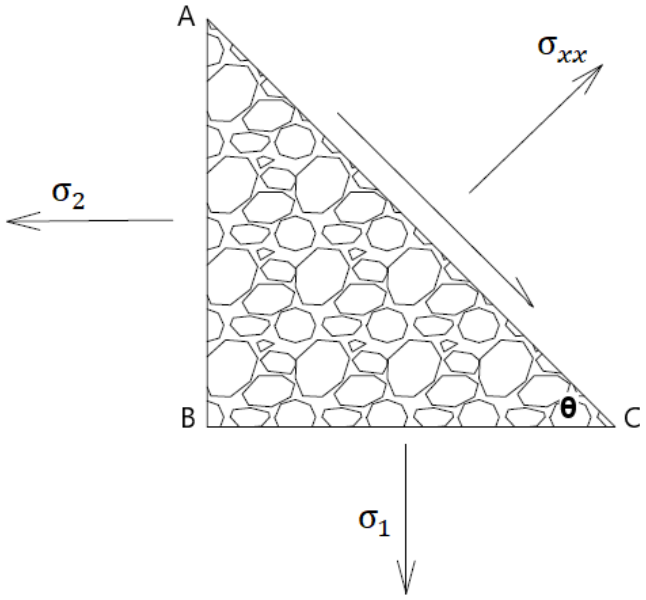

Figure 2-4 Diagram for derivation of Mohr's circle

Assuming that the soil mass is in equilibrium and summing all the forces in x-direction: $\sum F_x = 0$

$$\sigma_{xx}AC - \sigma_1 BC\cos\theta - \sigma_2 AB\sin\theta = 0$$

$$\sigma_{xx} - \sigma_1\, BC/AC\cos\theta - \sigma_2\, AB/AC\sin\theta = 0$$

From the figure,

$$\cos\theta = BC/AC \text{ and } \sin\theta = AB/AC$$

We get,

$$\sigma_{xx} = \sigma_1\cos^2\theta + \sigma_2\sin^2\theta$$

$$\sigma_{xy} = \sigma_1 - \sigma_2(\cos\theta\sin\theta)$$

Further, summing all the forces in y-direction,

We get,

$$\sigma_{xy} = \sigma_1 - \sigma_2(\cos\theta\sin\theta)$$

Further resolving using following trigonometric identities,

$$\cos^2\theta = {}^1/_2\,(1 + \cos 2\theta)$$

$$sin^2\theta = {}^1/_2\,(1 + \cos 2\theta)$$

$$\sin\theta\cos\theta = {}^1/_2 \sin 2\theta$$

Finally, we get the relationship,

$$\sigma_{xx} = (\sigma_1 + \sigma_2)/2 + (\sigma_1 - \sigma_2)/2\cos 2\theta$$

$$\sigma_{xy} = (\sigma_1 - \sigma_2)(\sin 2\theta)$$

These equations are for the Mohr's circle. They show the stress on any given plane with respect to the principal stresses.

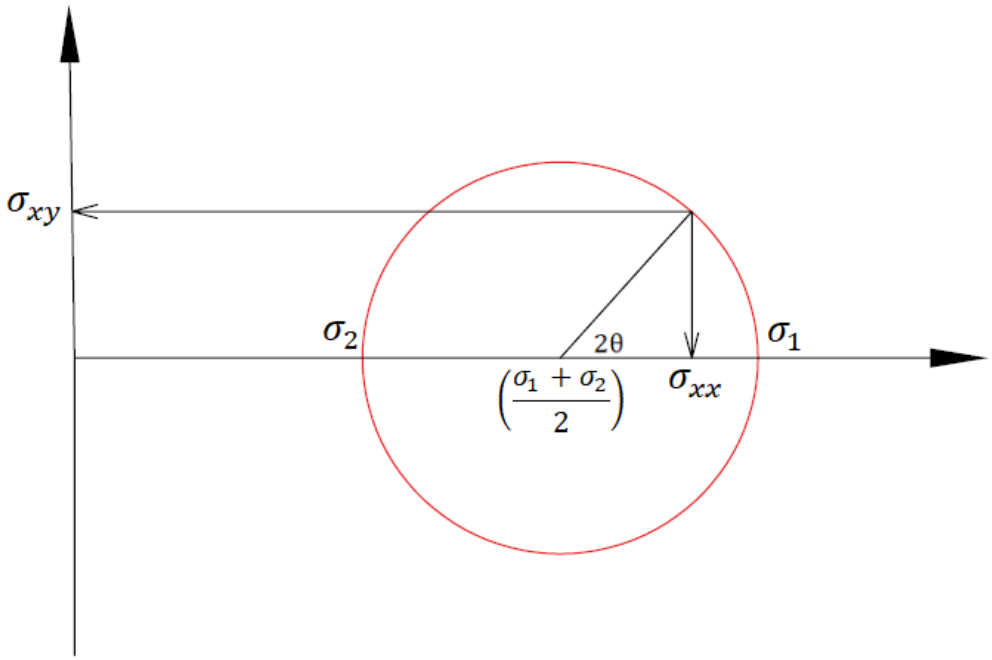

Figure 2-5: Mohr's circle derived from the equations

Chapter 3 Theory

3.1 Infinite slope theory

In infinite slope theory we consider a soil mass of thickness d which slips along the surface *x-x'* which is parallel to the ground surface and is making a slope angle of θ. The cross-section is shown in Figure 1. Here we also assumed a vertical distance '*a*' between the ground surface and the soil mass.

Then resolving both the axis,

$$a = d\cos\theta \tag{1}$$

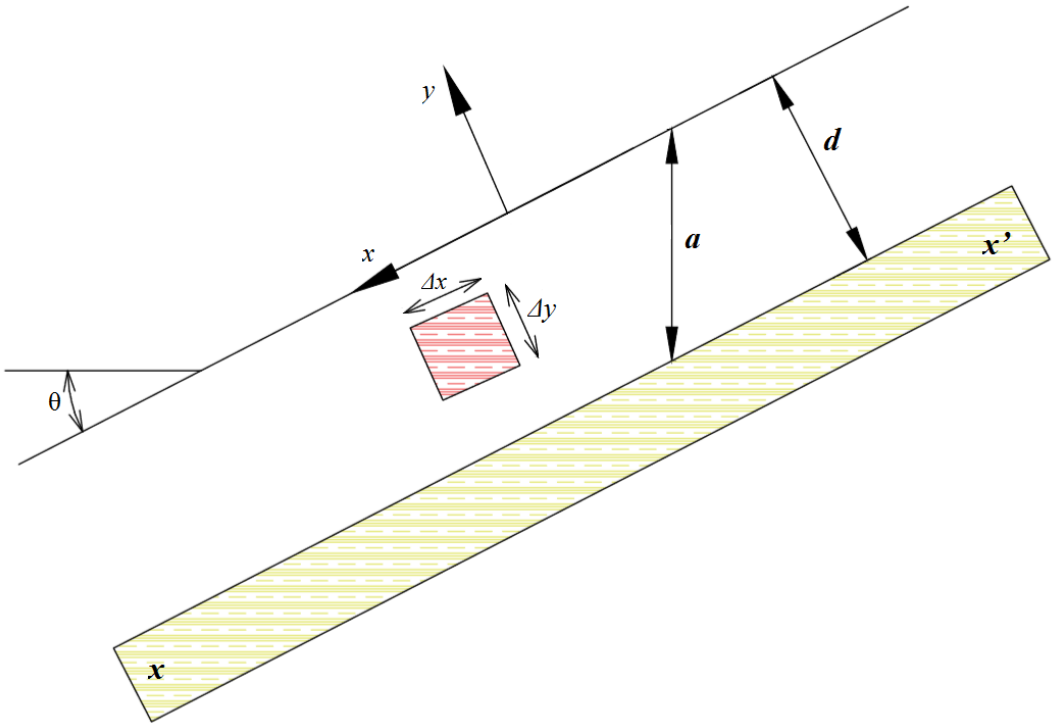

Figure 3-1: Diagram for infinite slope analysis

3.1.1 Stresses

Suppose we consider a small particle of soil with dimensions Δx and Δy. All the stresses and forces acting on the soil particle is shown in Figure 2 and Figure 3 respectively.

Therefore the total stress acting on the particles are:

$$\sigma'_{xx} = \sigma_{xx} + \frac{\partial \sigma_{xx}}{\partial x} \Delta x \quad (1.1a)$$

$$\sigma'_{yy} = \sigma_{yy} + \frac{\partial \sigma_{yy}}{\partial y} \Delta y \quad (1.1b)$$

$$\sigma'_{xy} = \sigma_{xy} + \frac{\partial \sigma_{xy}}{\partial x} \Delta x \quad (1.1c)$$

$$\sigma'_{yx} = \sigma_{yx} + \frac{\partial \sigma_{yx}}{\partial y} \Delta y \quad (1.1d)$$

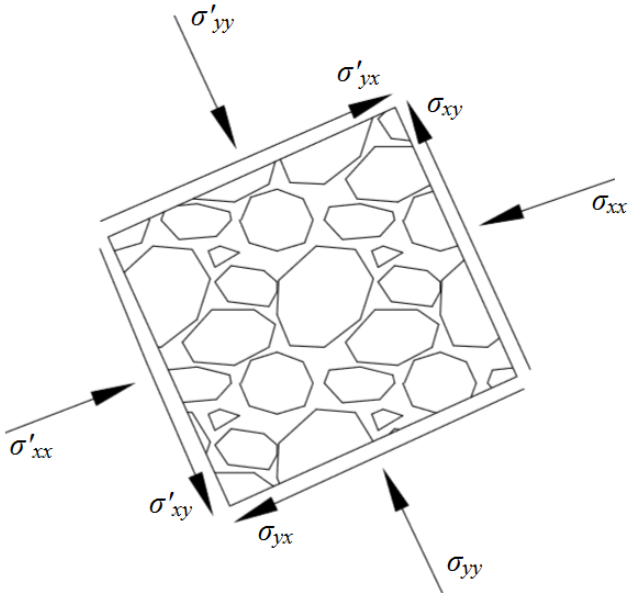

Figure 3-2: Stresses

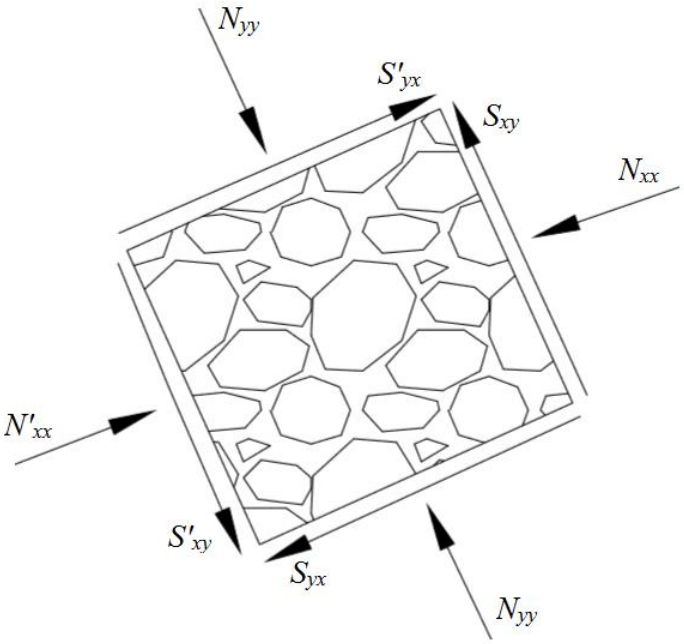

Figure 3-3: Forces

3.1.2 Forces

The forces acting on the soil particle are the normal forces *N* and the frictional forces *F* between the particles.

Therefor the total resolved forces acting on the particles are:

$$N_{xx} = \sigma_{xx}\,\Delta y \Delta z \quad (2.1a)$$

$$N'_{xx} = \sigma_{xx}\,\Delta y \Delta z \quad (2.1b)$$

$$N_{yy} = \sigma_{yy}\,\Delta x \Delta z \quad (2.1c)$$

$$N'_{yy} = \sigma_{yy} \Delta x \Delta z \quad (2.1d)$$

$$S_{xy} = \sigma_{xy}\,\Delta y \Delta z \quad (2.1e)$$

$$S'_{xy} = \sigma_{xy}\,\Delta y \Delta z \quad (2.1f)$$

$$S_{yx} = \sigma_{yx}\,\Delta x\Delta z \tag{2.1g}$$

$$S'_{yx} = \sigma_{yx}\,\Delta x\Delta z \tag{2.1h}$$

For static equilibrium, forces, F and moments, M must be equal to zero

$$\sum M = 0\,, \sum F_x = 0\,, \sum F_y = 0 \tag{2.2}$$

Summing all the moments and keeping the counter- clockwise a positive moment, we get

$$S'_{yx}\,\Delta y - S'_{xy}\,\Delta x - (N_{xx} - N'_{xx})\frac{\Delta y}{2} + \left(N_{yy} - N'_{yy}\right)\frac{\Delta x}{2} -$$

$$\gamma(\Delta x\Delta y\Delta z)\left[\frac{\Delta x}{2}\cos\theta + \frac{\Delta y}{2}\sin\theta\right] = 0 \tag{2.3}$$

Where the weight of soil particle is W,

$$W = \gamma(\Delta x\Delta y\Delta z) \tag{2.4}$$

Substituting eqs. (1.1) into eqs. (2.1) and the result in eq. (2.3), we get

$$\left(\sigma_{yx} + \frac{\partial\sigma_{yx}}{\partial y}\,\Delta y\right)(\Delta x\Delta y\Delta z) - \left(\sigma_{xy} + \frac{\partial\sigma_{xy}}{\partial x}\,\Delta x\right)(\Delta x\Delta y\Delta z) +$$

$$\frac{\partial\sigma_{xx}}{\partial x}\,\frac{\Delta x}{2}(\Delta x\Delta y\Delta z) - \frac{\partial\sigma_{yy}}{\partial y}\,\frac{\Delta y}{2}(\Delta x\Delta y\Delta z) - \gamma(\Delta x\Delta y\Delta z)\left[\frac{\Delta x}{2}\cos\theta + \frac{\Delta y}{2}\sin\theta\right] = 0 \tag{2.5}$$

Dividing each term in eq. (2.5) by the volume of the soil particle ($\Delta x \Delta y \Delta z$), and takin the limit as $\Delta x \to 0$ and $\Delta y \to 0$, we get

$$\sigma_{yx} - \sigma_{xy} = 0 \tag{2.6a}$$

$$\sigma_{yx} = \sigma_{xy} \tag{2.6b}$$

Summing all the forces in x- direction,

$$\sum F_x = N_{xx} - N'_{xx} + S_{yx} - S'_{yx} + W \sin\theta = 0 \tag{2.7a}$$

Substituting eqs. (1.1) into eqs. (2.1) and the result in eq. (2.7), we get

$$\sigma_{xx}\, \Delta y \Delta z - \left(\sigma_{xx}\, \frac{\partial \sigma_{xx}}{\partial x}\, \Delta x\right) \Delta y \Delta z + \sigma_{yx}\, \Delta x \Delta z -$$

$$\left(\sigma_{yx}\, \frac{\partial \sigma_{yx}}{\partial x}\, \Delta y\right) \Delta x \Delta z + \gamma (\Delta x \Delta y \Delta z) \sin\theta = 0 \tag{2.7b}$$

Again, dividing it by the volume of the soil particle ($\Delta x \Delta y \Delta z$), we get

$$\frac{\sigma_{xx}}{\Delta x} - \frac{\sigma_{xx}}{\Delta x} - \frac{\partial \sigma_{xx}}{\partial x} + \frac{\sigma_{yx}}{\Delta y} - \frac{\sigma_{yx}}{\Delta x} - \frac{\partial \sigma_{yx}}{\partial x} + \gamma \sin\theta = 0 \tag{2.7c}$$

Further resolving we have,

$$\frac{\partial \sigma_{xx}}{\partial x} + \frac{\partial \sigma_{yx}}{\partial x} = \gamma \sin\theta \tag{2.7d}$$

Similarly, summing all the forces in x- direction,

$$N_{yy} - N'_{yy} - W \cos\theta + S_{xy} - S'_{xy} = 0 \tag{2.8a}$$

Further resolving, finally we get,

$$\frac{\partial \sigma_{yy}}{\partial y} + \frac{\partial \sigma_{xy}}{\partial x} = -\gamma \cos\theta \tag{2.8b}$$

Eqs. (2.9b & 2.10b) can be written ad differential equations as stresses cannot change in x-direction, this gives us

$$\frac{d\sigma_{yx}}{d_y} = \gamma \sin\theta \tag{2.9a}$$

$$\frac{d\sigma_{yy}}{d_y} = -\gamma \cos\theta \tag{2.9b}$$

From eq. (2.4) we can also say,

$$\frac{d\sigma_{yx}}{d_y} = \frac{d\sigma_{xy}}{d_y} \tag{2.10}$$

Integrating eqs. (2.7), we get,

$$\sigma_{xy} = y\,\gamma \sin\theta + C_o \tag{2.11a}$$

$$\sigma_{yy} = -y\,\gamma \cos\theta + C_1 \tag{2.11b}$$

Here, C_o and C_1 are arbitrary constants and these constants can be zero since the shear stress and normal stress are zero at ground surface

$$\sigma_{xy} = y\gamma \sin\theta \tag{2.12a}$$

$$\sigma_{yy} = -y\,\gamma \cos\theta \tag{2.12b}$$

The relationship in eqs. (2.12) shows the equilibrium condition of any material. If the condition is not satisfied, then the material can be said it is out of equilibrium.

3.2 Finite element method

In the present research work, finite element analysis of the soil sample was carried out. The different material properties of the soil was found out in our laboratory along with different literatures published are used for this analysis. The results obtained through the finite element modelling are further discussed below. Finite element method (FEM) is a powerful alternative approach for soil stability which is quite accurate and requires few prior assumptions, especially when it comes to the failure mechanism. It may be valuable when the geometries are generally ill shaped and are difficult to solve using conventional methods. The graphical and mesh representation allows us to better visualize the failure mechanism. Researchers like (Griffiths, D.V., et al, 1999) had used FEM for slope stability analysis and obtained good solutions.

Different material parameters for the soil like elastic modulus, Young's modulus, Poisson's ratio, porosity, Cohesion, angle of internal friction are given in Table 3-1.

Table 3- 1: Material parameters for soil slope

Material parameters	Values
Young's modulus	1×10^5 kN/m^2
Poisson's ratio	0.4
Porosity	0.3
Cohesion	1.019 kPa
Angle of internal friction	0.64228 rad

Chapter 4 Laboratory experiment

The laboratory experiment was conducted in a box setup called sandbox which is fitted with a motor for the circulation of water. The dimensions of the sandbox are 250cm long, 60cm wide and 80 cm in height with glass walls in each side as shown in figure-1. The sandbox consisted of the sections, section(a) in the extreme left act as a reservoir from where the water was released to another section. Section(b) in the middle stores the sample for conducting the experiment. Section(c) in the extreme right is the water storage area from where the collected water was again transferred to the section(a) using the motor. Several potential failure surfaces are formed leading to deep catastrophic collapse as the pore water pressure on the soil sample increases. According to the model, the simulation can efficiently evaluate critical conditions and the hydraulic computation can reasonably resolve the potential failure surface. Once the failure surface is yielded, a discontinuous joint is added on the geometry of the model to simulate the discontinuous deformation behaviour of the structure.

4.1 Experiment setup

The sandbox was levelled and was kept parallel to the ground. A soil sample was compacted with given cohesion, c and internal friction, ϕ and a

trapezoidal structure was made in the section(b). Below the section(b) three pore water pressure and three soil pressure meters were installed and this setup was connected to a data logger and all the received data was stored in a data storage. A modified camera was also installed at a height focusing on the sample to record the deformation and the movement of soil mass when the experiment starts.

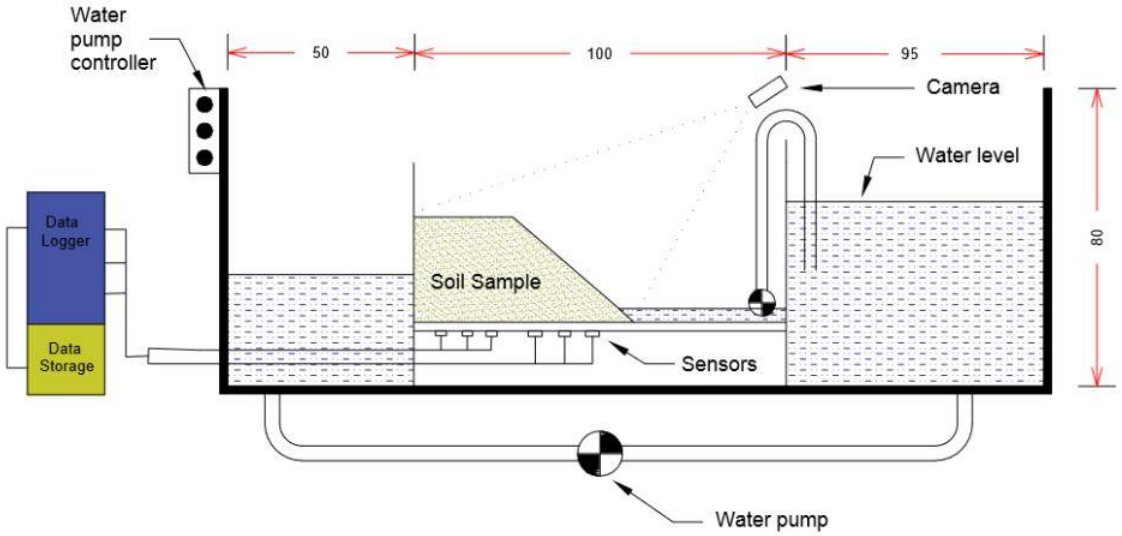

Figure 4-1: Laboratory sandbox setup diagram

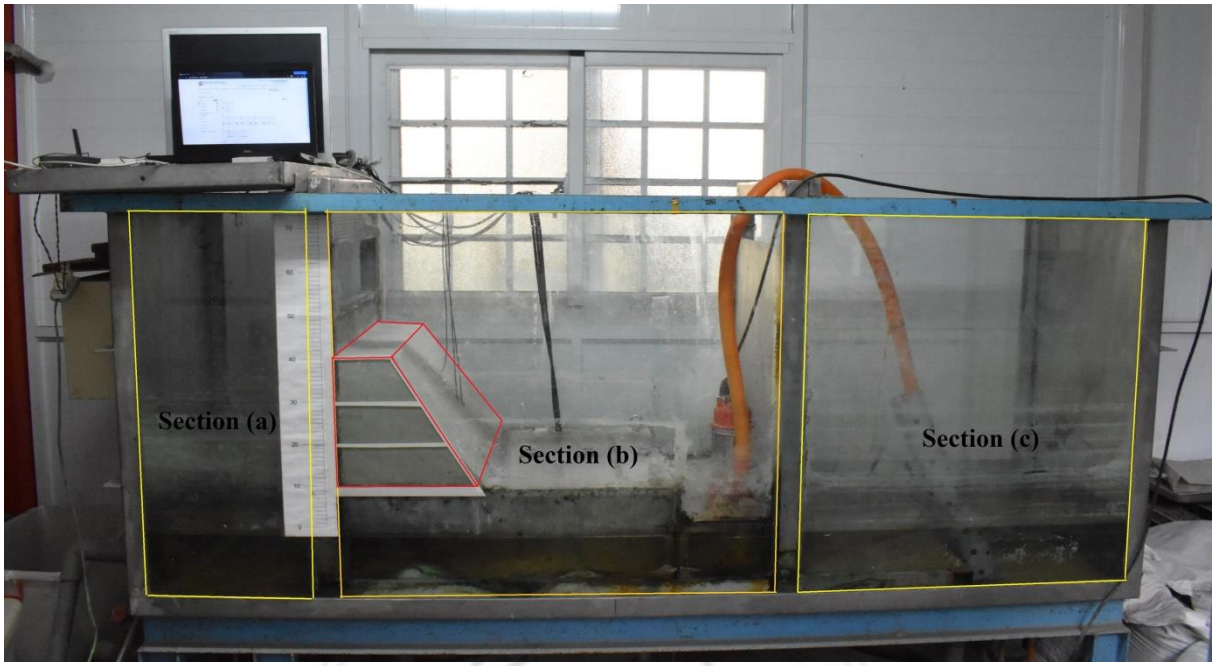

Figure 4-2: Actual experimental setup

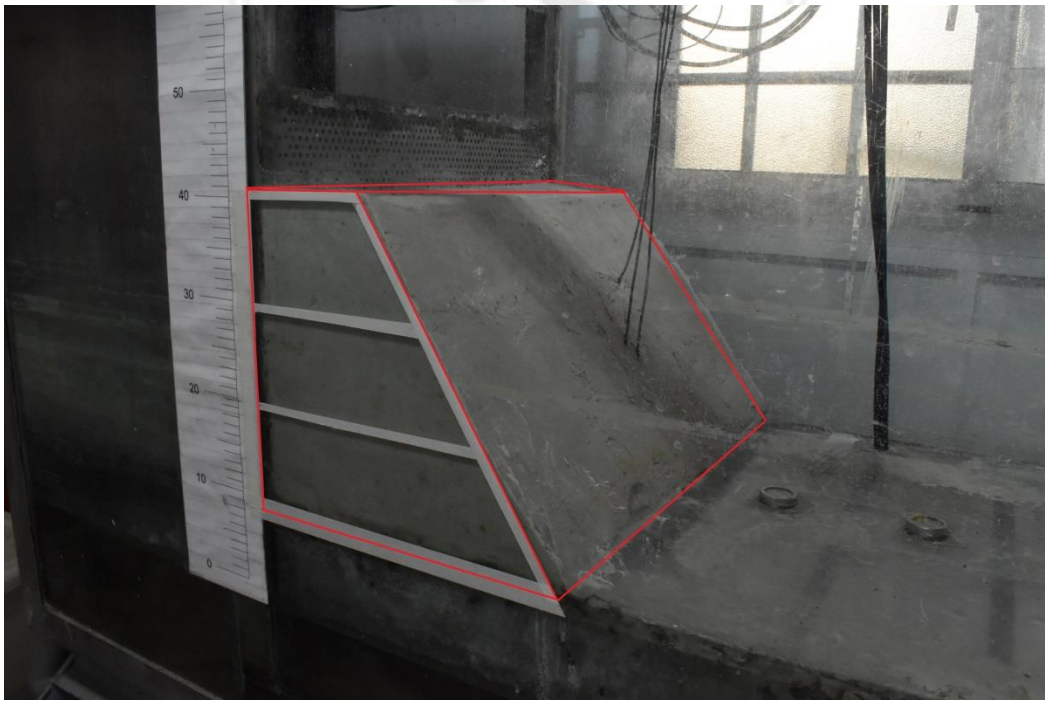

Figure 4-3: Cross section of the sample

Figure 4-4: Cross section of the sample with foam balls to capture the movement of landslide

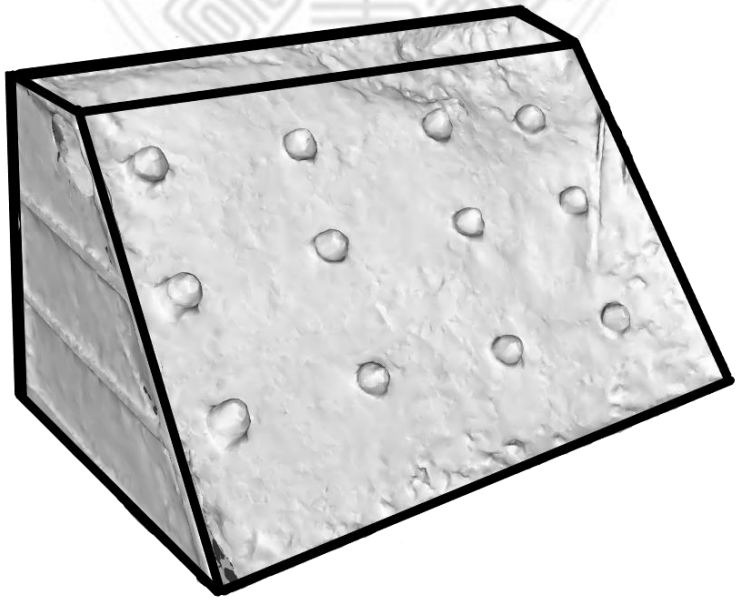

Figure 4-5: X-ray of the Cross section of the sample with foam balls

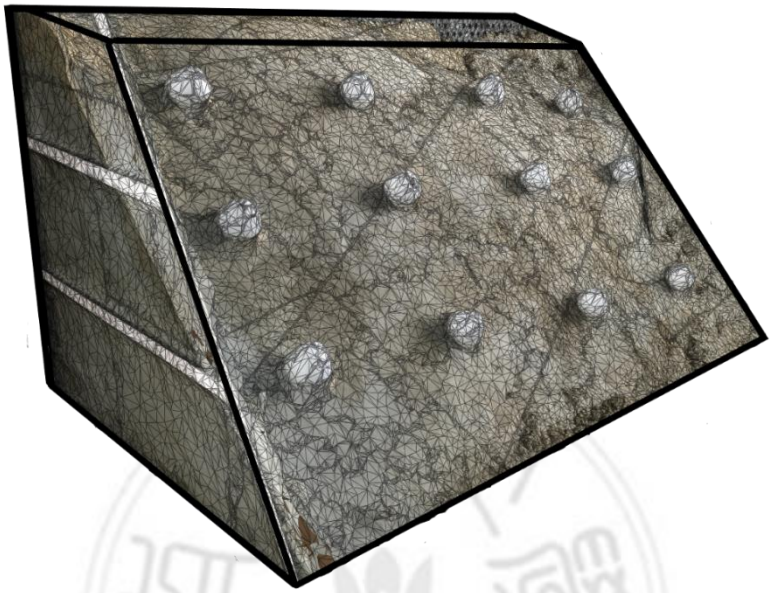

Figure 4-6: Cross section of the sample divided in mesh

4.2 Soil characteristics

The soil used in this experiment is uniform silica sand of D_{50}= 0.195 mm taken from a dammed lake located in Chiufenerhshan, Nantou county, Taiwan.

The main significance of calibration is to check the given sensors (soil pressure & pore pressure meter) that are consistent with our assumptions. The best way to achieve this is to obtain relations by using laboratory equipment

utilizing materials with known constitutive relationships. Real-life landslides cannot be considered for model calibration as the timing of real-life landslides are unknown nor the details of motion are sufficiently known to us. The laboratory experiment was carried out in our lab in a laboratory setup called 'sandbox'. The setup allowed the flow of mass when the pore water pressure increased in the sand mass along a path and simulate the lateral spreading controlled by internal stresses. A simulation software, COMSOL was used to produce the contour maps of moving sand masses. The objective of the calibration is to compare certain parameters obtained by the models with the observation. The parameters include the rise in pore water pressure in the sand mass, the mass of sand displaced, etc.

Table 4- 1: Mechanical and hydraulic characteristics of the material used in the experiment.

Sample	D_{50} (mm)	C_u	C_c	ϕ
Silica sand	0.195	1.826	1.253	37

D_{50} = median grain size; C_u = coefficient of uniformity; C_c = coefficient of curvature; ϕ = angle of internal friction in degrees.

4.3 Laboratory experiment apparatus

3 Pore pressure meters and 3 soil pressure meters were connected to the data receiver (I-7016D) and data stored in an embedded system (5231M).

<1>Pore pressure meter: 3 pore pressure meters (KPA-200KPA) shown in the figure were used. These transducer measure pore water pressure recommendable voltage excitation voltage. If desired, they can be used as pressure-based underground water level transducers by installing then in the well. It uses an input voltage of 5V. The output voltage is directly proportional to the level of water.

<2>Soil pressure meter: 3 soil pressure meters (BEE-A-200KP) shown in the figure were used. These are soil pressure transducers that are used most popularly in measuring fields. It can also measure dynamic soil pressure caused by an earthquake or landslide. It uses an input voltage of 5V. The output is directly proportional to the weight of the soil above the sensor.

Table 4- 2: Specifications of all the sensors and the embedded system.

Name	**Model number**	**Voltage**
Pore-water pressure meter	BPB-A-200KP	5V
Soil pressure meter	BEE-A-200KP	5V
Data receiver	I-7016D	24V
Data storage	5231-M	24V

4.4 Connection of Instruments

The connection of Pore pressure meter, Soil pressure meter, data receiver and the voltage regulator was done as shown in the diagram below:

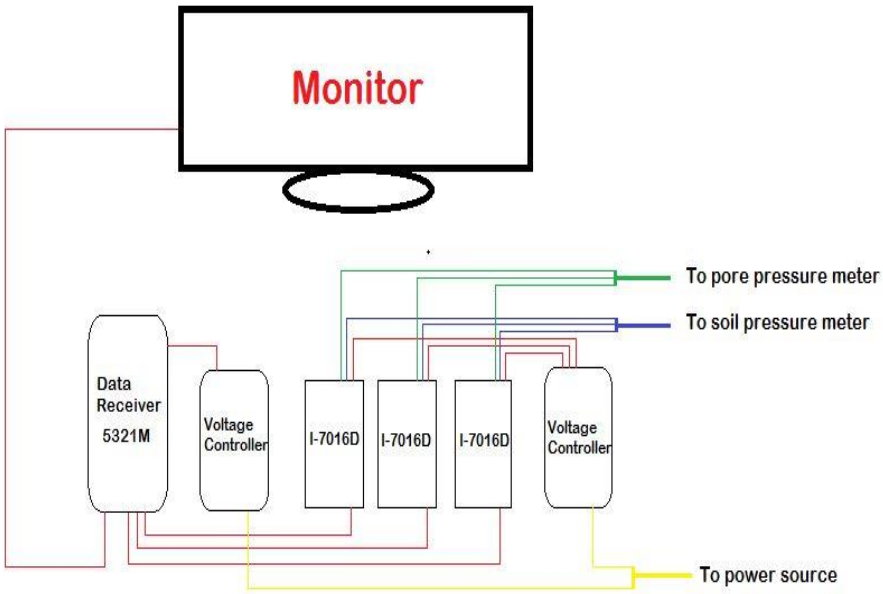

Figure 4-7: Line diagram of all the connections

Figure 4-8: Experimental sensor connection

4.5 Calibration of sensors

The main significance of calibration is to check the given sensors (soil pressure & pore pressure meter) that are consistent with our assumptions. The best way to achieve this is to obtain relations by using laboratory equipment utilizing materials with known constitutive relationships. Real-life landslides cannot be considered for model calibration as the timing of real-life landslides are unknown nor the details of motion are sufficiently known to us. The laboratory experiment was carried out in our lab in a laboratory setup called ‘sandbox’. The setup allowed the flow of mass when the pore water pressure increased in the sand mass along a path and simulate the lateral spreading controlled by internal stresses. A simulation software, COMSOL was used to produce the contour maps of moving sand masses. The objective of the calibration is to compare certain parameters obtained by the models with the observation. The parameters include the rise in pore water pressure in the sand mass, the mass of sand displaced, etc. For the calibration of sensors, initial readings were taken and accordingly a graph was plotted and from that graph, the linear equation was found out accordingly.

Pore pressure meter

The relation between the Ground water level (H_w) and voltage (R_w) is expressed with an equation of a straight line which can be written $H_w = A \times R_w + B$, where A and B are constants.

Table 4- 3: Constant values for the calibration of pore water pressure meter

Number of pore pressure meter	A	B
W1	56.547	1.974
W2	55.946	1.4837
W3	52.910	1.5103

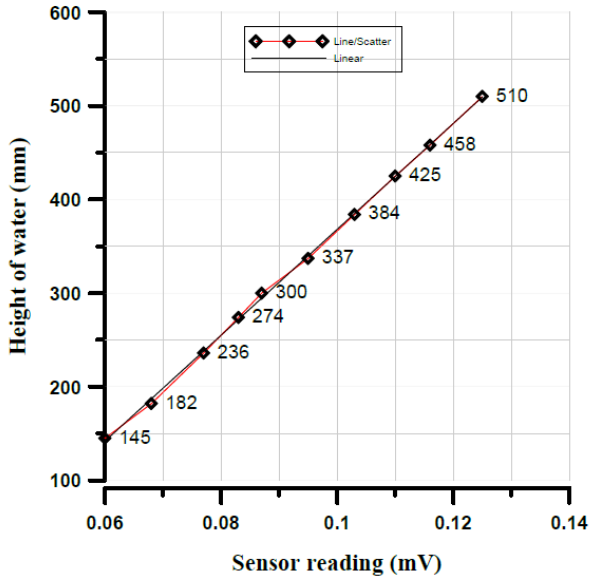

Figure 4-9: Graph for pore pressure meter-1 (W)

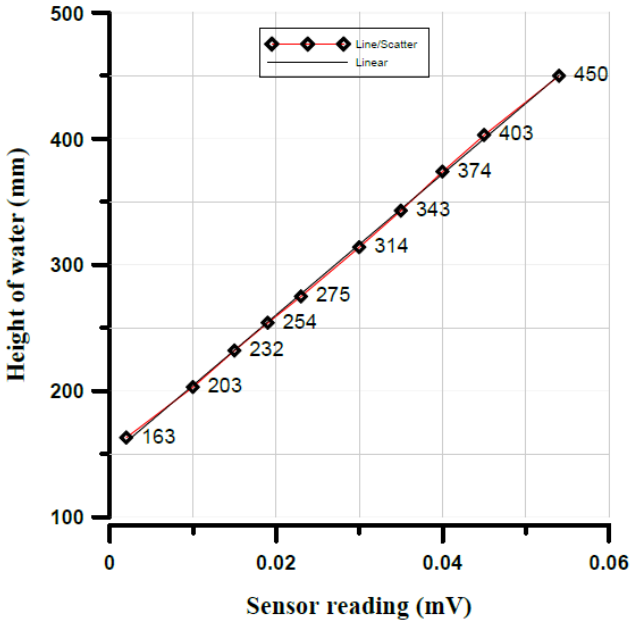

Figure 4-10: Graph for pore pressure meter-2 (W2)

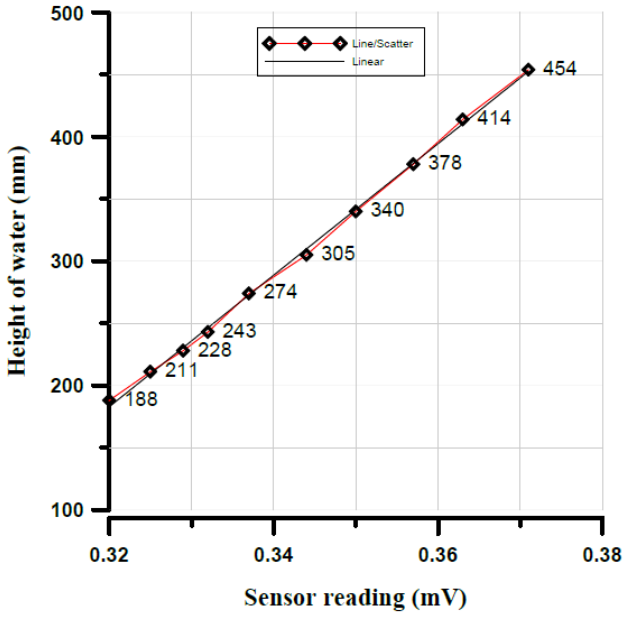

Figure 4-11: Graph for pore pressure meter-3 (W3)

Soil pressure meter

The relation between the Weight of soil (H_s) and voltage (R_s) is expressed with an equation of a straight line which can be written $H_s = A \times R_s + B$, where A and B are constants.

Table 4- 4: Constant values for the calibration of soil pressure meter.

Number of soil pressure meter	A	B
S1	40580	14183
S2	44383	195051
S3	44528	158250

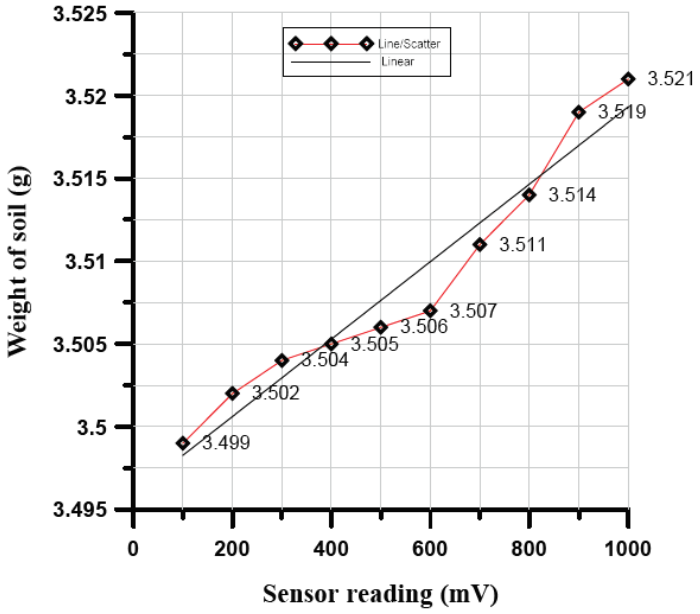

Figure 4-12: Graph for soil pressure meter-1 (S1)

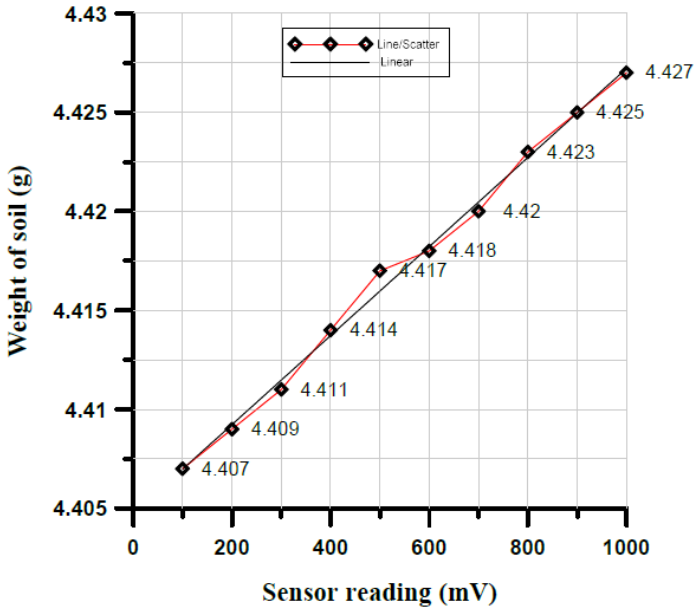

Figure 4-13: Graph for soil pressure meter-2 (S2)

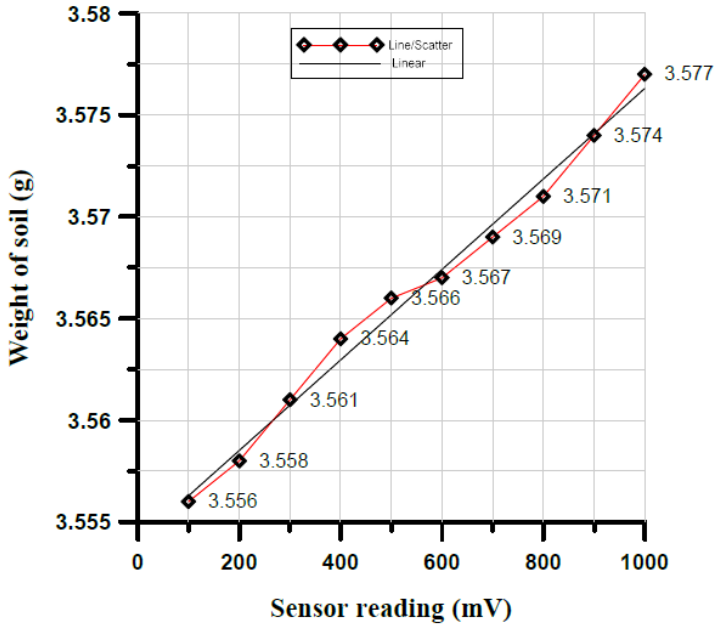

Figure 4-14: Graph for soil pressure meter-3 (S3)

Chapter 5 Experiment verification

5.1 Using a Finite element analysis software i.e. COMSOL

The above laboratory experiment was verified using a Finite element analysis software i.e. COMSOL. The study in COMSOL is done on two parameters. For the porous medium and subsurface flow, Darcy's Law was chosen and for the study of solid medium solid mechanics was chosen. Some parameters were pre-assumed as mentioned below.

Table 5- 1: Pre-assumed parameters for COSOL

Expression	**Value**
Length of sample (Left)	0 cm
Length of sample (Top)	8 cm
Length of sample (Right)	35 cm
Height of sample	26 cm
Water level	25 cm
Possible seepage height	1 cm
Young's modulus	1E8 N/m^2
Poisson's ratio	0.4
Soil density	2000 kg/m^3
Water density	1000 kg/m^3
Porosity	0.3
Cohesion	1.019 kPa
Friction angle for saturated soil	0.64228 rad
Friction angle for unsaturated soil	0.5236 rad
Factor of safety	1

5.2 Failure simulation in COMSOL

During the simulation process, three studies were done simultaneously. In first Darcy's Law was computed to get the pore pressure profile. In the second study, the slope is simulated in account with hydrostatic pressure and gravity. In the third study, the pore pressure and initial stress generated from the first and second studies respectively were studied. Further external stress and initial stress and strain were also added followed by the Mohr-Coulomb criterion to study the electro-plastic failure of soil. The 2D geometry was constructed in COMSOL and the water levels were marked using the point command. Two materials were chosen for the study of Darcy's law. Material 1 and material 2 were soil and water respectively. Two pressure head boundaries were allotted in the geometry.

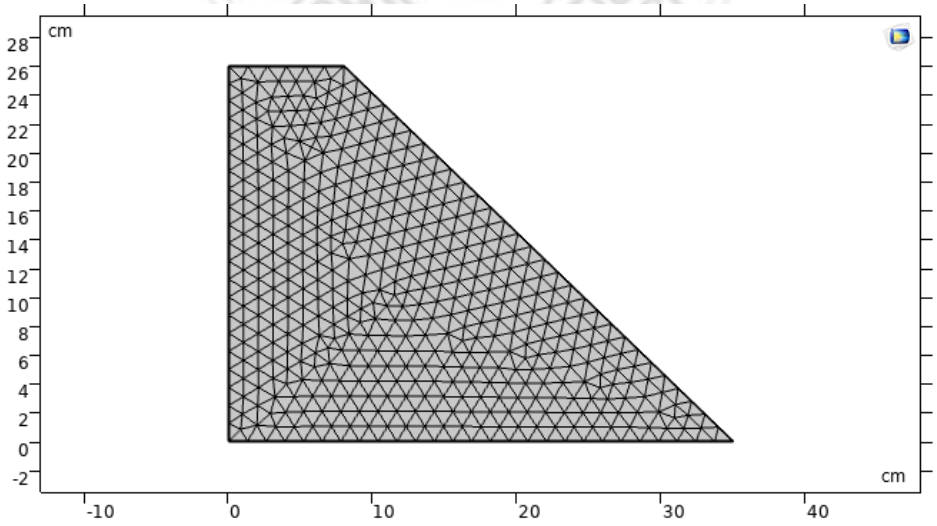

Figure 5-1: Physics controlled mesh diagram of the soil sample.

Chapter 6 Discussions

6.1 Finite element analysis

This study shows that laboratory experiments (sandbox) and numerical model (finite element method) can be combined to obtain more accurate and detailed results for the deformation in soil. The experiment shows that the seepage mechanism in slope mass that is comprised of unsaturated homogeneous and cohesion-less materials is influenced by the geometry of the soil mass. In this study, the stability of soil mass was studied and the laboratory experiment was verified using the COMSOL Multi-physics software. Two materials were added for the simulation, Fluid material, and porous material. Darcy's law was studied to obtain the pore pressure and the flow of fluid in porous medium. The overall stability of the slope was studied using the Mohr-Coulomb criterion for electro-plastic analysis. The study also shows that the stability of the soil mass depends on the type of soil present in that area, the geometry of the soil, the material composition of the soil mass. Cohesion, C and angle of internal friction, ϕ also plays a major role in the stability of soil mass.

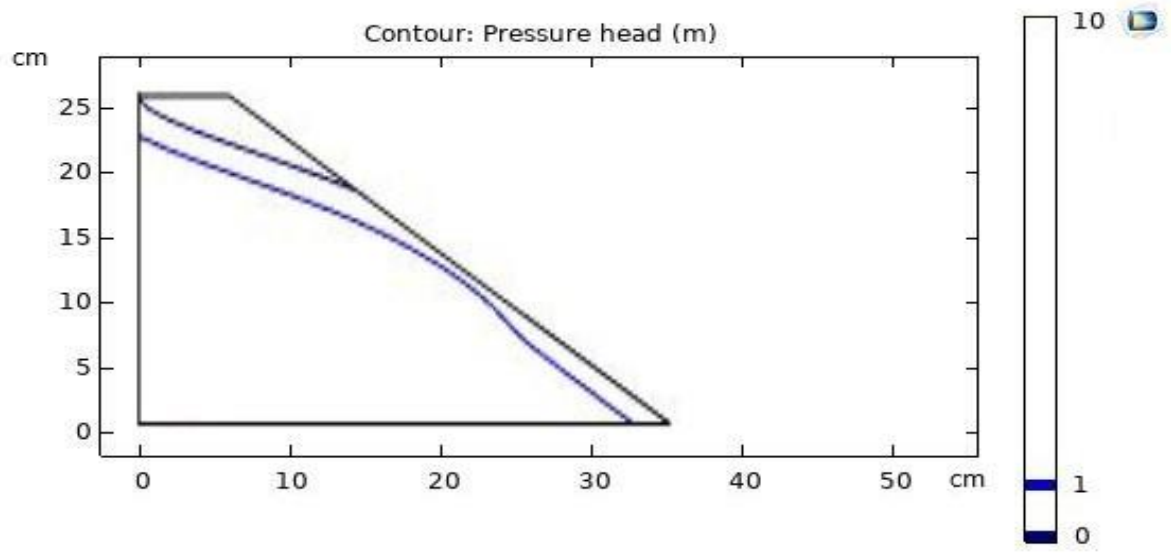

Figure 6-1: Pressure head in soil sample

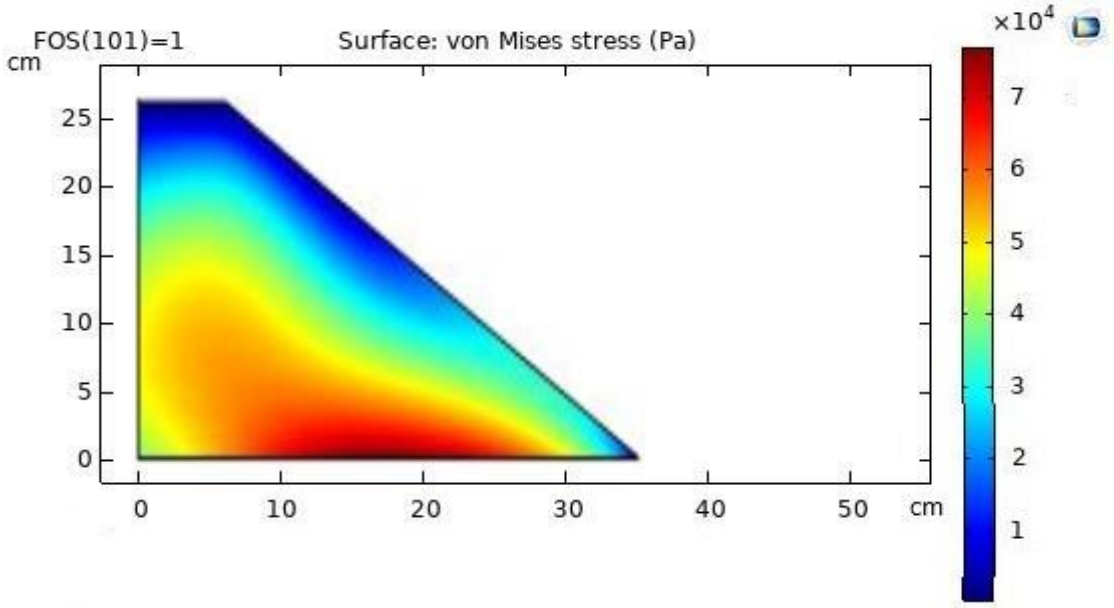

Figure 6-2: von Mises stress diagram in the soil sample

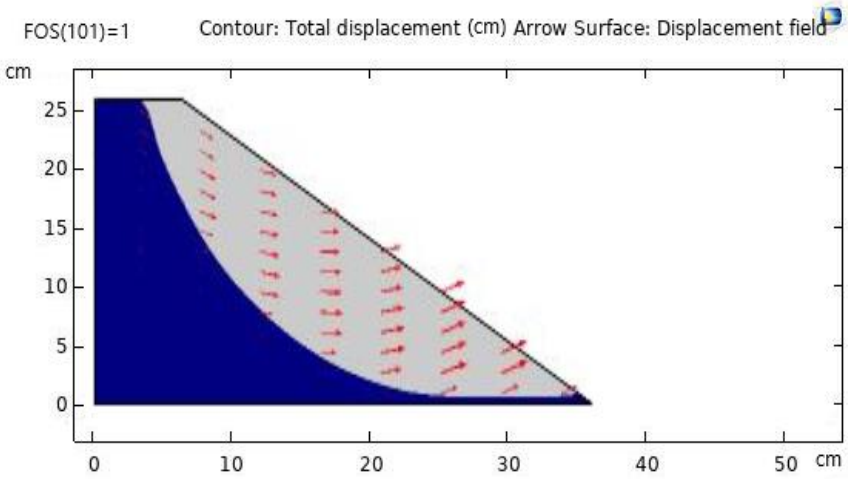

Figure 6-3: Effective plastic strain just before the failure of soil sample

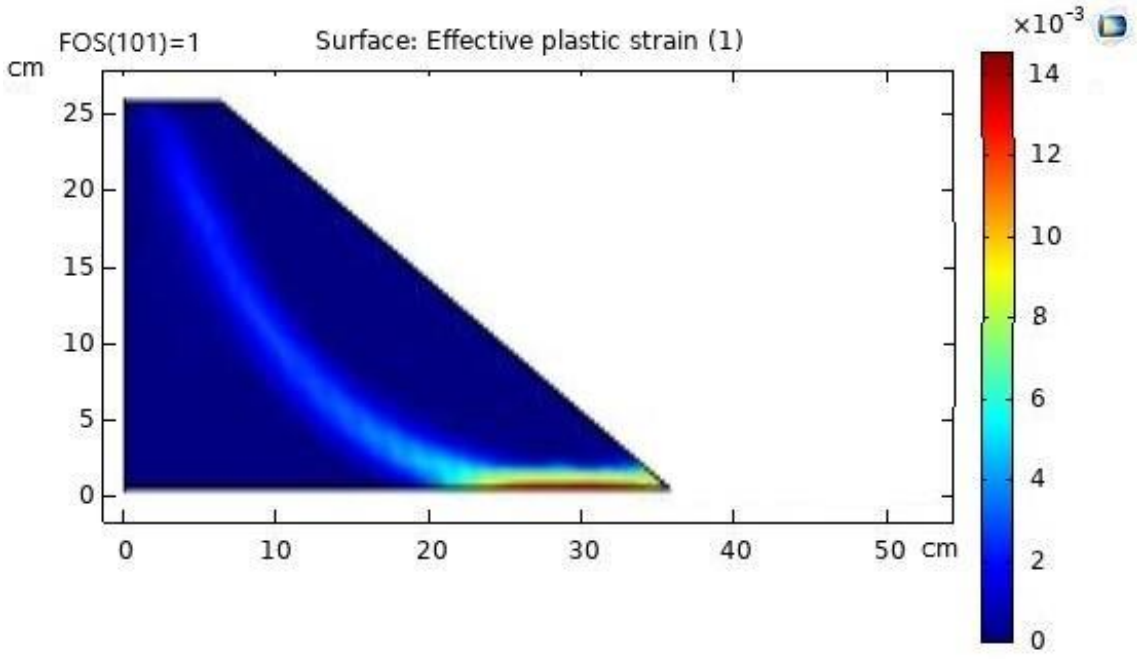

Figure 6-4: Slip circle just before the collapse.

6.2 Approval of slope failure

When the water level in the soil mass started to increase, the voids in the soil particles started to fill with the water. This lead to the soil movement and the variation in ground-water. The graph obtained after the laboratory experiment in sandbox clearly shows the start in the rise of the pore- water pressure and after few minutes as the groundwater level reaches the initiation of seepage flow there is a loss in soil mass and hence the groundwater level also decreases. As the seepage flow continues to transport some water, the graph still shows an increase in the ground water level. But as soon as the groundwater level reaches its critical value, there is a sudden displacement of soil mass with water and hence here the landslide occurs.

(a)

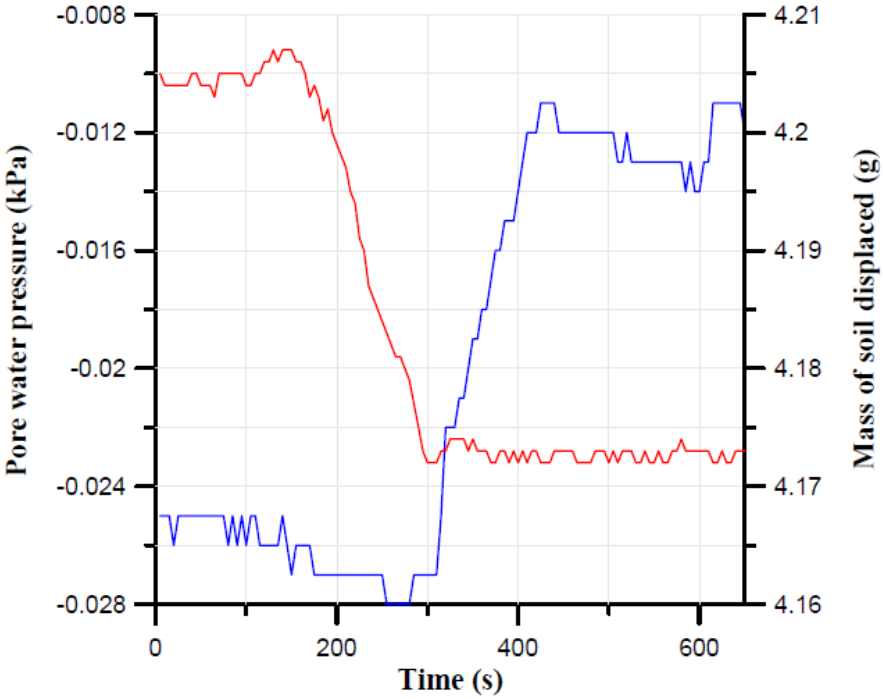
-0.008
-0.012
-0.016
-0.02
-0.024
-0.028
Pore water pressure (kPa)
4.21
4.2
4.19
4.18
4.17
4.16
Mass of soil displaced (g)
0
200
400
600
Time (s)

(b)

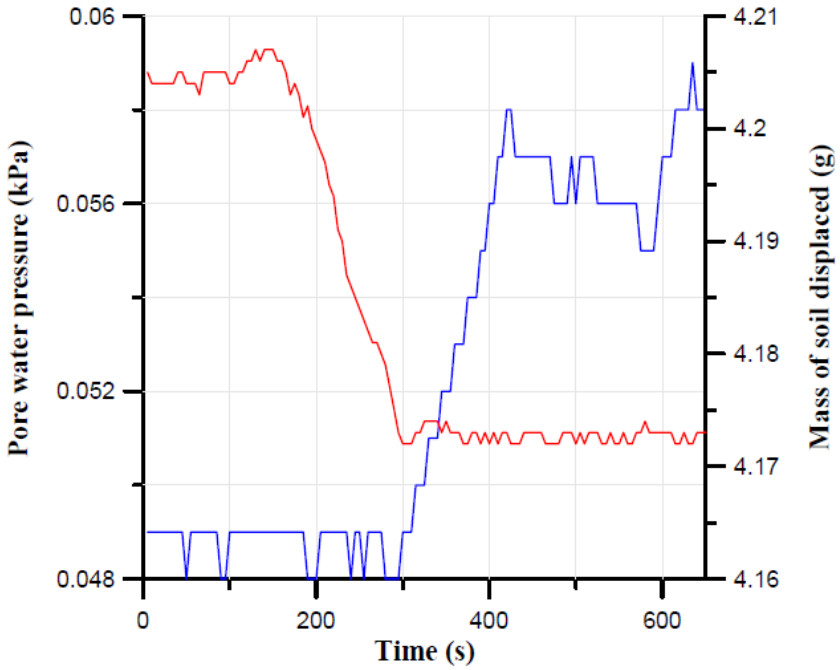
0.06
0.056
0.052
0.048
Pore water pressure (kPa)
4.21
4.2
4.19
4.18
4.17
4.16
Mass of soil displaced (g)
0
200
400
600
Time (s)

(c)

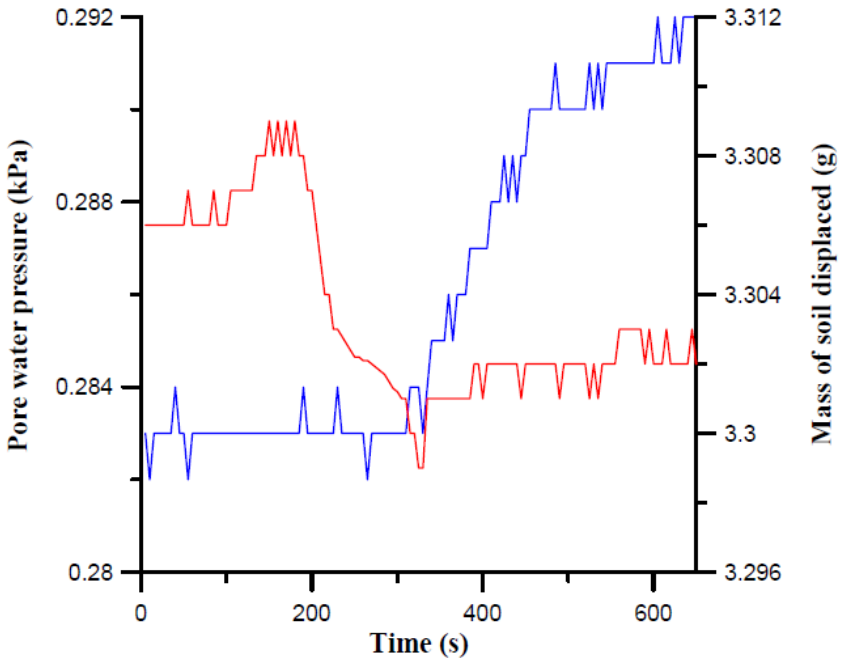

Figure 6-5: Evolution of pore water and sliding of soil mass in laboratory experiment.

As the above graph clearly shows that the there is a constant seepage of fluid material to the soil particles and after some time when all the air voids are completely replaced with water, there is a rise in water level. As the water level keeps on increasing, after some time there is a sudden fall in the graph. It clearly shows that at that particular time there is a sudden movement of the fluid material. The same graph also shows that there is a constant line which indicated that there is no displacement of any soil mass and suddenly after some time there is another

fall in the graph and again the graph becomes constant. This shows that there is a movement of soil slope which simulates that the landslide has occurred.

The simulation shows that as the toe of the slope is submerged in water the shear zone is initiated ad tends to extend throughout the slope. As the slip surface gradually develops, the strength of the soil mass also decreases from the peak to the toe, and the slip surface propagates within the landslide. Hence the simulation of the model in numerical modelling software validates the above laboratory experiment.

Chapter 7 Conclusion

In this study, a soil slope has been simulated by a finite element software considering two different studies, Darcy's law and solid mechanics.The results obtained by this method have been analyzed and the simulation has been found to be alligned to the results in the laboratory. The factor of safety put in the simulation was 1.

Moreover, further research should be done in which a mixture of different types of soils and sediment sizes should be combined to see the behaviour of different combinations of soil profiles. Different soil profiles can be analysed in the laboratory following the above study. As different countries have different geographic locations and the types and profiles of soil differ from place to place. This study can be used for the detailed study of different types of soil profiles. We can further combine different soil types to make a new soil profile in the laboratory. The displacement properties and characteristics of this new soil type are unknown. This above study is the perfect and suitable way to analyze the detailed deformation characteristics in the laboratory.

This study can be evaluated further to develop some mechanisms combined with programming to develop some sensors to install in such high-risk areas, anywhere in the world to get an early warning before a major landslide reducing the risk to the lives of human beings.

Reference

1. Beliaev, A. Y., & Kozlov, S. M. (1996). Darcy equation for random porous media. Communications on pure and applied mathematics, 49(1), 1-34.
2. Brown, G. O. (2002). Henry Darcy and the making of a law. Water Resources Research, 38(7), 11-1.
3. Chae, B. G., Lee, J. H., Park, H. J., & Choi, J. (2015). A method for predicting the factor of safety of an infinite slope based on the depth ratio of the wetting front induced by rainfall infiltration. Natural Hazards & Earth System Sciences, 15(8).
4. Drucker, D. C., & Prager, W. (1952). Soil mechanics and plastic analysis or limit design. Quarterly of applied mathematics, 10(2), 157-165.
5. Chen, X. P., Zhu, H. H., Huang, J. W., & Liu, D. (2016). Stability analysis of an ancient landslide considering shear strength reduction behaviour of slip zone soil. Landslides, 13(1), 173-181.
6. Griffiths, D. V., & Lane, P. A. (1999). Slope stability analysis by finite elements. Geotechnique, 49(3), 387-403.
7. Hungr, O. (1995). A model for the runout analysis of rapid flow slides, debris flows, and avalanches. Canadian Geotechnical Journal, 32(4), 610-623.

8. Iverson, R. M. (2000). Landslide triggering by rain infiltration. Water resources research, 36(7), 1897-1910.
9. Kanungo, D. P., Pain, A., & Sharma, S. (2013). Finite element modeling approach to assess the stability of debris and rock slopes: a case study from the Indian Himalayas. Natural hazards, 69(1), 1-24.
10. Labuz, J. F., & Zang, A. (2012). Mohr–Coulomb failure criterion. Rock mechanics and rock engineering, 45(6), 975-979.
11. Lin, H. C., Kan, Y. C., Sung, W. P., & Hong, Y. M. (2015). A deep catastrophic failure model of hillslope for numerical manifold method and multiple physics computation. Arabian Journal for Science and Engineering, 40(3), 735-746.
12. Moore, J. R., Boleve, A., Sanders, J. W., & Glaser, S. D. (2011). Self-potential investigation of moraine dam seepage. Journal of Applied Geophysics, 74(4), 277-286.
13. Okeke, A. C. U., & Wang, F. (2016). Critical hydraulic gradients for seepage-induced failure of landslide dams. Geoenvironmental Disasters, 3(1), 9.
14. Prancevic, J. P., Lamb, M. P., Palucis, M. C., & Venditti, J. G. (2018). The Role of Three-Dimensional Boundary Stresses in Limiting the Occurrence and Size of Experimental Landslides. Journal of Geophysical Research: Earth Surface, 123(1), 46-65.

15. Sarkar, K., Singh, T. N., & Verma, A. K. (2012). A numerical simulation of landslide-prone slope in Himalayan region—a case study. Arabian Journal of Geosciences, 5(1), 73-81.
16. Sarkar, K., & Singh, T. N. (2007). Evaluation of Instability Analysis of Slope: A Numerical Approach. Mining Engineering Journal, 8(10), 11-31.
17. Singh, T. N., Verma, A. K., & Sarkar, K. (2010). Static and dynamic analysis of a landslide. Geomatics, Natural Hazards and Risk, 1(4), 323-338.
18. Varnes, D. J. (1978). Slope movement types and processes. Special report, 176, 11-33.
19. Wang, G., & Sassa, K. (2003). Pore-pressure generation and movement of rainfall-induced landslides: effects of grain size and fine-particle content. Engineering geology, 69(1-2), 109-125.
20. Yao-Ming Hong, The Piping Erosion of subsurface Flow using a Laboratory Experiment. J. Appl. Sci. & Agric., 9(11): 186-189, 2014.